12th International Symposium on Turbulence and Shear Flow Phenomena (TSFP12)
Osaka, Japan (Online), July 19-22, 2022

# REYNOLDS NUMBER EFFECTS IN 2D SQUARE-BAR ROUGHNESS WALL-BOUNDED TURBULENT FLOWS

**Jiahao Kong**
School of Mechanical Engineering
University of Adelaide
Adelaide, 5005 South Australia, Australia.
jiahao.kong@adelaide.edu.au

**Luke G. Bennetts**
School of Mathematical Sciences
University of Adelaide
Adelaide, 5005 South Australia, Australia.

**Bagus Nugroho**
Department of Mechanical Engineering
University of Melbourne
Melbourne, 3010 Victoria, Australia

**Rey Chin**
School of Mechanical Engineering
University of Adelaide
Adelaide, 5005 South Australia, Australia.

## ABSTRACT

Turbulent boundary layers (TBLs) above two-dimensional (2D) square-bar roughness are studied experimentally to investigate Reynolds number effects on the turbulent flow properties at moderate friction Reynolds numbers ($Re_\tau$). Previous studies have examined 2D square-bar roughness at low $Re_\tau$ numerically and high $Re_\tau$ experimentally. Inspired by their results, a set of experiments were conducted for a classical k-type 2D roughness with the pitch $p$ to height $k$ ratio $p/k = 8$, at $Re_\tau = 1840,\ 3900$ and 4950. The roughness effect increases with increasing $Re_\tau$ and extends to the wake region in terms of the streamwise turbulence intensity. The results shows that the drag coefficient $C_f$ converges for the fully-rough, indicating that it behaves like a classical k-type roughness at a fully-developed state when it reaches $Re_\tau \geq 3900$ with $\delta_{99}/k \geq 53$.

## INTRODUCTION

Turbulent boundary over a rough surface is an important component in many engineering applications because it can influence heat, mass and momentum transfer, and drag coefficient $C_f$ (Chung *et al.*, 2021). There are various types of roughness pattern in the literatures, such as sand grain type roughness, riblets, etc. One type of roughness that has attracted plenty of attention in the last 60 years is 2D regularly distributed roughness (or simply 2D roughness), which is known to have spanwise-aligned roughness elements with constant streamwise spacing $p$. Review studies by Raupach *et al.* (1991) and Jiménez (2004) indicate that many surface roughness patterns, particularly the sand grain type (or "k-type") obeys Townsend's outer-layer similarity hypothesis (Townsend, 1974). The hypothesis states that above the roughness sublayer and at a sufficiently large Reynolds number, turbulent flows are independent of the configuration of surface roughness. In order to obey the similarity hypotheses however, Jiménez (2004) suggested caveats that the roughness pattern need to have boundary layer height and roughness height ratio of $\delta_{99}/k \geq 40$ and $Re_\tau \geq 4000$. Here $Re_\tau = \delta_{99} U_\tau/\nu$, where $\nu$ is kinematic viscosity and $U_\tau$ is friction velocity. The friction velocity is defined as $U_\tau = \sqrt{\tau_w/\rho}$, where $\tau_w$ is the wall shear stress and $\rho$ is the fluid density.

Although many roughness indeed obey Townsend's outer-layer similarity hypothesis, many 2D roughness studies have shown a contradictory view on the similarity hypothesis, particularly for developing boundary layers (Krogstad & Antonia, 1999; Lee & Sung, 2007; Volino *et al.*, 2011). For 2D square-bar roughness, direct numerical simulation (DNS) results (Lee & Sung, 2007) showed that the 2D roughness effect extends to the outer region ($y/\delta_{99} \geq 0.5$) for TBLs with $\delta_{99}/k = 22$ at, $Re_\tau \approx 500$ (a relatively low Reynolds numbers). Intrigued by these opposing views, Efros & Krogstad (2011) performed a 2D square-bar roughness boundary layer experiment over a wide range of Reynolds numbers ($Re_\tau = 4,200$ – $13,300$) to investigate the roughness effects in the outer region at high $Re_\tau$, and high boundary layer height and roughness height ratio $\delta_{99}/k \approx 130$. Their results indicate that the outer-layer similarity hypothesis is preserved, stipulating that an increase in scale separation ratio and Reynolds number provide a different conclusion for 2D roughness flow. From the discussion above, it is clear that Reynolds numbers $Re_\tau$ and the ratio of TBL thickness to the roughness height $\delta_{99}/k$ play significant roles for the validity of the wall-similarity hypothesis in 2D roughness TBLs. Moreover, these two parameters will also affect the drag coefficient $C_f$

For 2D square-bar roughness, they are known to experience increases in drag with $p/k$, where it reaches the maximum drag at $p/k = 8$. Beyond this value, the drag starts do decrease. For $p/k = 8$, the DNS results of (Lee & Sung, 2007) shows $C_f \approx 0.012$ for a low $Re_\tau$ TBL flow, while the high $Re_\tau$ experiment (Efros & Krogstad, 2011) resulting in $C_f = 0.0068$ for TBLs at $Re_\tau \geq 9900$. In addition, Djenidi *et al.* (2018) conducted a TBL study over 2D circular-rod roughness at a range of Reynolds numbers, $620 \leq Re_\tau \leq 7000$, and reported $C_f \approx 0.007$ at the highest $Re_\tau$, which is close to the result of Efros & Krogstad (2011). However, to the best of the authors' knowledge, there are not many studies that investigate 2D square-bar roughness TBLs at moderate Reynolds numbers, $600 \leq Re_\tau \leq 9000$. To reduce the uncertainty caused by different cross-sectional shapes, there is a need to exam-

ine TBLs over a similar roughness as Lee & Sung (2007) and Efros & Krogstad (2011) at moderate $Re_\tau$.

In the present report, we investigate the influence of Reynolds numbers on 2D roughness on the turbulence statistics at moderate $Re_\tau$. Hot-wire anemometry (HWA) TBL experiments are performed at Reynolds numbers $Re_\tau =$ 1840, 3900 and 4950 over 2D square-bar roughness $p/k = 8$, which is similar to the studies of Lee & Sung (2007) and Efros & Krogstad (2011). The present study reports the post-processing approach, including the determination and validation of the friction velocity $U_\tau$. Finally, the mean statistics and drag coefficient for the rough wall data are analyzed.

## EXPERIMENTAL METHOD

In this study, the Cartesian coordinates $x$ and $y$ refer to streamwise and wall-normal directions, respectively. The corresponding velocity components are $u$ and $v$, and $\delta_{99}$ denotes the wall-normal location where the mean streamwise velocity is 99% of the free-stream velocity, $U_\infty$. The superscript $+$ indicates viscous scale normalization so that, for instance, $U^+ = U/U_\tau$ and $y^+ = y \times U_\tau/\nu$, where $U_\tau$ is the friction velocity.

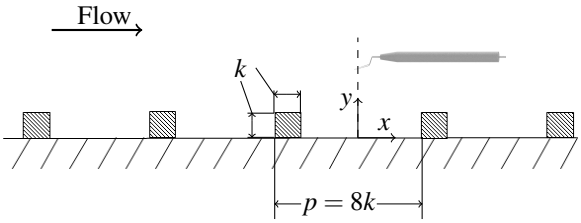


Figure 1. Schematic views of square-roughened surfaces and the measurement location

## EXPERIMENT CONDITION

Experiments were performed in a closed-loop wind tunnel at the University Adelaide. The test section was 2 m long and had a rectangular cross-sectional area of $0.5 \times 0.3\,\mathrm{m}^2$. The sidewalls were adjusted to maintain zero pressure gradient (ZPG) along the test section with a range of free-stream velocities, $6 \le U_\infty \le 20\ \mathrm{m\,s^{-1}}$, for the smooth and rough wall measurements. For various free-stream speed flows, the acceleration parameter, defined as $K = \frac{\nu}{U_\infty^2}\frac{\partial U_\infty}{\partial x}$, was less than $5 \times 10^{-9}$ (Volino *et al.*, 2009). The bottom wall of the test section was fully covered by a flat aluminum plate to serve as the smooth wall for the baseline flow measurement. The boundary layer was tripped near the leading edge of the aluminum plate with tripping devices, consisting of a 3 mm diameter threaded rod and a 36 grit sandpaper of 100 mm in length to reach a fully-developed state. A smooth wall measurement was conducted with the tripping devices at $Re_\tau = 1900$ to act as a baseline case. The smooth wall TBL has the shape factor $H = \delta_*/\theta = 1.357$, where $\delta_*$ is the displacement thickness and $\theta$ is the momentum thickness, which shows a good agreement with the criterion value of $H$ introduced by Chauhan *et al.* (2009) at corresponding $Re_\tau$, and indicates the smooth wall TBL reaches a fully-developed state.

The smooth wall TBL measurement was made at 1.5 m downstream of the tripping device with a free-stream speed of $20\,\mathrm{m\,s^{-1}}$ to achieve a friction Reynolds number, $Re_\tau = 1900$. For the rough-wall measurements, the rough surface was made by affixing ABS plastic square bars spanwisely on the aluminum plate downstream of the tripping device. Figure 1 shows a schematic view of the arrangement of the square bars. The bar height was k=1.5 mm, and the streamwise spacing was $p = 8k$, similar to the numerical and experimental studies (Lee & Sung, 2007; Efros & Krogstad, 2011). The spacing value of $p = 8k$ is specifically chosen because the drag increases with $p/k$ and it reaches the maximum drag at $p/k = 8$. The rough-wall measurements were taken over a range of free-stream velocities, $6 \le U_\infty \le 16\,\mathrm{m\,s^{-1}}$ at a fixed streamwise location. The position is identical to the smooth wall measurement, which is also in the middle of two adjacent roughness bars, as shown in Figure 1. The experimental conditions for the smooth- and rough-wall measurements are summarized in Table 1.

The TBL profiles were measured with hot-wire anemometry (HWA) sensors and taken from the near-wall position to the free-stream flow at $y = 1.5\delta_{99}$ by using a 1D traverse system. Note that this study defines $y$ as the wall-normal distance from the bottom wall for rough wall measurements, as shown in Figure 1. The traverse system comprised a Mitutoyo height gauge, driven by a stepper motor and controlled by an optical linear encoder, which has a resolution of $30\,\mu$m. The HWA sensors were single-wire boundary-type probes, operated by an in-house built hot-wire anemometry. The probes had a tip spacing of 2 mm. Wollaston wires were soldered to the prong tips etched to expose a sensor filament of $d = 2.5\,\mu$m diameter and $l = 0.51$ mm length. The length-to-diameter ratio of the sensor filament was $l/d \ge 200$, which satisfies the suggestion by Ligrani & Bradshaw (1987) to minimize attenuation due to end conduction. The velocity signal from HWA was sampled with frequency $f_s = 51200$ Hz and a duration $T = 120$ s using a National Instrument data acquisition board (USB-NI6211). As shown in Table 1, the viscous sample time interval, defined as $t^+ = 1/f_s(U_\tau^2/\nu)$, is less than 3 to capture all the relatively high energy content frequency (Hutchins *et al.*, 2009). Note that the largest scales of turbulent structures are observed to exceed $20\delta$ (Adrian *et al.*, 2000), hence, the sampling duration is required to encompass several hundreds of these large-scale events for the converged statistics ($TU_\infty/\delta_{99} > 20000$).

The hot-wire sensors were statistically calibrated against a Pitot tube located above the hot-wire probes, approximately 10 mm into the free-stream flow. Calibrations were made before and after each traverse. The free-stream velocity was determined by the difference between the total and static pressures from the Pitot tube and monitored by an electronic barometer (220DD Baratron, MKS). The temperature condition was also monitored by a RTD-type thermocouple (PT1000) to compensate for the drift of the HWA signal caused by temperature. Fourth-order polynomial curves were used to fit the pressure data and hot-wire voltage signals. Linear interpolation was made to correct the temperature drift between pre- and post-calibration. In addition, the free-stream velocity was recorded throughout each traverse station and used to compare with the hot-wire signals in the free-stream flow. The whole data set was discarded if the difference of $U_\infty$ from the pressure data and hot-wire signals is larger than $\pm 1\%$ (Hutchins *et al.*, 2009).

### Estimating $U_\tau$

Two methods were used to find $U_\tau$ indirectly for the smooth- and rough-wall data for the present streamwise velocity measurements. The composite profile method of Chauhan *et al.* (2007) was used to determine $U_\tau$ and $\Pi$ simultaneously for the smooth-wall data, where $\Pi$ is known as the wake pa-

Table 1. The smooth and rough wall experiment condition

| Case | Sym | $p/k$ | $x$ | $U_\infty$ | $Re_\tau$ | $\delta_{99}/k$ | $C_f$ | $l^+$ | $t^+$ | $TU_\infty/\delta_{99}$ |
|---|---|---|---|---|---|---|---|---|---|---|
| | | | m | (ms$^{-1}$) | | | $\times 10^{-3}$ | | | |
| smooth | ○ | – | 1.5 | 20 | **1900** | – | 2.8 | 25 | 0.71 | 62 |
| Ref 1 | — | – | 3.75 | 20 | **3470** | – | 2.49 | 24.5 | 0.51 | 17 |
| Ref 2 | — | – | 6.3 | 20 | **4780** | – | 2.34 | 25.3 | 0.48 | 15 |
| pk8A | □ | 8 | 1.5 | 6 | **1840** | 49 | 7.9 | 12.76 | 0.185 | 9.9 |
| pk8B | □ | 8 | 1.5 | 12.8 | **3900** | 53 | 6.9 | 24.7 | 0.72 | 19.2 |
| pk8C | □ | 8 | 1.5 | 16 | **4950** | 53.3 | 6.9 | 31.6 | 1.13 | 24 |

Ref 1 and Ref 2 refer to Marusic *et al.* (2015).

rameter. The method uses all measurement points to fit with the reference profile. The reference profile is based on a composite function comprising the Musker function for the inner region and an exponential function for the wake region. Those equations can be found in Sections II – III of Chauhan *et al.* (2007). The composite profile method was compared with the Clauser method (Clauser, 1954), which involves forcing the mean velocity profile to fit onto a pre-defined log law by adjusting $U_\tau$ as

$$U^+ = \frac{1}{\kappa}\ln(y^+) + B, \tag{1}$$

where $\kappa$ and $B$ are known as the von Karman constant and the intercept constant, which are suggested as 0.39 and 4.3 for the smooth wall TBL Chauhan *et al.* (2009); Marusic *et al.* (2015); Squire *et al.* (2016). The fitting process also requires properly defined bounds of the log region, which are suggested at $y^+_{inner} = 3\sqrt{Re_\tau}$ and $y^+_{outer} = 0.15Re_\tau$ for the smooth-wall TBL following Marusic *et al.* (2013). The resulting $U_\tau$ between the two methods is very similar, with a difference of less than 2%. In Figure 2, the smooth-wall velocity and turbulence intensity profiles, scaled by two $U_\tau$ from the above methods, are compared with the result of the DNS study (Chan *et al.*, 2021) at a similar Reynolds number $Re_\tau \approx 1900$. Two velocity profiles show a good agreement with the DNS result at all positions. The turbulence intensity profiles also show an excellent collapse with the DNS profiles above the log region ($y^+ \geq 100$). In the following discussions, the smooth-wall TBL case is normalized by the $U_\tau$ that is obtained from the composite method.

For the rough-wall flow cases, there are three additional unknowns in the normalized mean velocity profile, namely the von Karman constant $\kappa$, the roughness offset $\varepsilon$ and the Hama roughness function $\Delta U^+$ (Perry & Joubert, 1963). Based on the knowledge of 2D roughness TBL velocity profiles from Leonardi *et al.* (2003) and Lee & Sung (2007), we assumed $\kappa = 0.41$ for rough-wall measurements. The offset $\varepsilon$ accounts for the effect that the roughness displaces the entire flow away from the bottom wall. In this study, the wall-normal position from the virtual origin of the mean velocity profile is defined as $y' = y - \varepsilon$. The classic method to obtain $U_\tau$, $\varepsilon$, and $\Delta U^+$ was via the modified Clauser method (Perry & Joubert, 1963), which requires the knowledge of the bounds of the log region. Here we follow Perry & Li (1990) to optimize $\varepsilon$ via iteration on the modified Clauser method. In this method, $U/U_\infty$ is plotted as a function of $(y-\varepsilon)/\delta^*$, where $\delta^*$ is the displacement boundary layer thickness. In this profile, the equation for the log region is

$$\frac{U}{U_\infty} = \frac{1}{\kappa}\frac{U_\tau}{U_\infty}\ln\left(\frac{y-\varepsilon}{\delta^*}\right) + C, \tag{2}$$

where $C = f(\frac{U_\tau}{U_\infty}, \Pi)$ is the intercept constant of the line (Perry & Li, 1990). By adding $\varepsilon$ to the experimental data to adjust the virtual origin from the bottom wall ($\varepsilon = 2/k$) to the crest of roughness ($\varepsilon = -2/k$), several iterations were made by applying the first-order polynomial fit to evaluate a constant line. The constant line providing the least square error fitting to the experimental data within the log region is considered the best fit line, where the log region is defined from $y^+ = 3.4\sqrt{Re_\tau}$ to $y/\delta = 0.19$ for rough-wall TBLs (Squire *et al.*, 2016). The initially estimated $U_\tau$ can be determined from the slope of the constant line, and the optimized offset value $\varepsilon$ was applied to determine the wall-normal position $y'$.

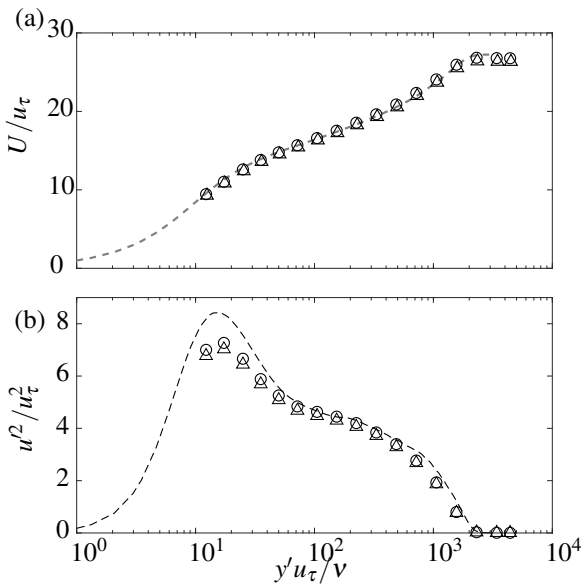


Figure 2. Comparison of the present smooth wall profiles scaled by $U_\tau$ from two methods and the DNS smooth wall results at $Re_\tau \approx 1900$ (Chan *et al.*, 2021). (a) inner-scaled mean velocity profile; (b) inner-scaled turbulence intensity profile. Dash line, the DNS smooth wall result; circle, the present result from the composite method; triangle, the present result from the Clauser method.

The accuracy of $U_\tau$ estimated via the modified Clauser method (for the rough wall cases) has been investigated by Flack *et al.* (2007), and they found that it has uncertainty around 3 – 5%. To minimise this uncertainty, a novel technique that relies on the outer-layer similarity hypothesis (Townsend, 1974) was introduced by Monty *et al.* (2011) (from here on it is referred to as the 'defect' method) and it is used to 'improve' the $U_\tau$ estimated from the modified Clauser method. The $U_\tau$ estimation was made by fitting the velocity defect profile ($U^+_\infty - U^+$ vs $y'/\delta_{99}$) onto the smooth-wall data from the lower bound of the outer region, $y'/\delta_{99} \approx 0.1$. The mean velocity and defect profiles for the 2D rough wall TBLs at $Re_\tau = 1840$ and 4950 normalized by the $U_\tau$ from the modified Clauser method and defect method were plotted in Figure 3. The comparison shows that the differences in terms of $U_\tau$ and $\Delta U^+$ between the two methods are small, which are about 4% and 2%, respectively. These differences are well within the expected error as indicated by Flack *et al.* (2007) and Schultz & Myers (2003). Moreover, velocity defect profiles for the rough wall cases collapse well with the corresponding smooth wall case, indicating agreement with the outer-layer similarity hypothesis. Due to this, the improved estimation technique, which is a combination of the modified Clauser method used to obtain $\varepsilon$ and the defect method used to determine $U_\tau$ and

$\Delta U^+$, is used for all 2D roughness data.

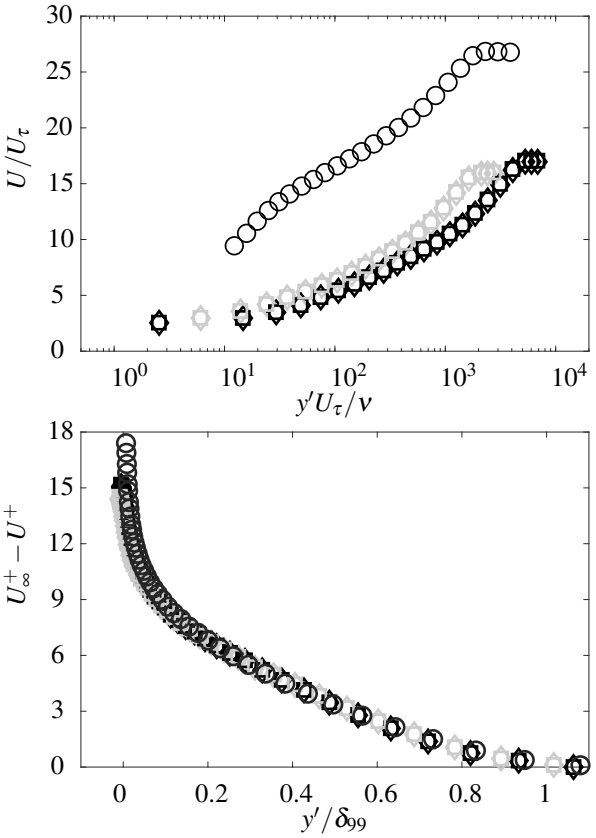


Figure 3. Comparison in estimating $U_\tau$ of 2D roughness at $Re_\tau = 1840$ and 4950 using the modified Clauser method (Diamond) and the defect method (Square). The result of rough-wall case at $Re_\tau = 3900$ is not shown here for brevity. As the reference profile for the defect method, the smooth wall TBL at $Re_\tau = 1900$ (open circle) is also plotted. Mean velocity profiles (a) and velocity defect profiles (b).

## VALIDATION

Alfredsson & Örlü (2010) introduced a diagnostic plot as $u'/U_\infty$ vs $U/U_\infty$ to prove the data quality without estimating $U_\tau$ for the smooth-wall measurement, where $u'$ is the local (root mean square) velocity fluctuation. The success of the diagnostic tool extended to the wall-bounded flows over roughness by considering $\Delta U^+$ (Castro *et al.*, 2013). The modified diagnostic plot is $u'/U'$ vs $U'/U'_\infty$, where $U' = U + \Delta U$, $U'_\infty = U_\infty + \Delta U$ and $\Delta U = \Delta U^+ \times U_\tau$. In this plot, the rough-wall TBL profiles collapse onto the smooth-wall result ($\Delta U = 0$) in the outer layer. Figure 4 plotted all rough-wall profiles with the smooth-wall result. The smooth-and rough-wall profiles show a good collapse on the dashed line for $0.6 \leq U'/U'_\infty \leq 0.9$. This observation indicates the smooth- and rough-wall TBLs in this study have a good quality in terms of the local mean velocity and velocity fluctuating, and shows agreement of the value of $\Delta U^+$ estimated from the improved technique.

## RESULT AND DISCUSSION

Figure 5 shows the distribution of mean velocity and turbulence intensity profiles on the 2D rough wall with $p/k = 8$

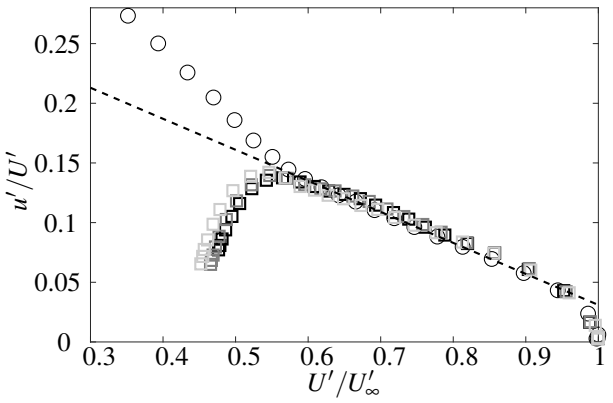


Figure 4. The modified diagnostic plot for all rough-wall measurements at $Re_\tau = 1840 - 4950$ (light to dark square) and the smooth-wall result (circle). Dashed line: the empirical line determined from the linear region of the smooth-wall data of Castro *et al.* (2013).

at Reynolds numbers $Re_\tau = 1840$, 3900 and 4950 (light to dark grey). As the baseline flows, the smooth wall TBLs of $Re_\tau = 1900$, 3470 and 4780 are also plotted with the rough wall cases (where the two high $Re_\tau$ cases are taken from Marusic *et al.* (2015)). Figure 5(a) shows inner-scaled mean velocity profiles, and clearly indicates the downward shift $\Delta U^+$ for the rough-walled case relative to the smooth-walled case. The effect of the surface roughness on the mean velocity distribution can be expressed in the mean velocity equation for the logarithmic layer, as

$$U^+ = \frac{1}{\kappa}\ln\frac{(y+\varepsilon)U_\tau}{\nu} + B - \Delta U^+. \quad (3)$$

The inner-scaled turbulence intensity plots are shown in Figure 5(b). As baseline flows, the smooth wall cases have a near-wall peak at $y^+ = 15$, indicating the highly energetic near-wall cycle of streaks and quasi-streamwise vortices (Kline *et al.*, 1967). For the rough wall cases, the magnitude of the inner peak diminishes from $Re_\tau = 1840$ to 3900 and the reduction reaches a maximum at $Re_\tau \geq 3900$. Note that the hot-wire spatial resolution for those two lower $Re_\tau$ cases has $l^+ \leq 25$, which is higher than the smooth wall TBLs and indicates that the spatial attenuation effect is negligible (Hutchins *et al.*, 2009). Hence, the absence of the inner peak is generally associated with the disturbance of the near-wall cycle of streaks and quasi-streamwise vortices near the surface roughness (Schultz & Flack, 2007; Monty *et al.*, 2011; Djenidi *et al.*, 2018). The reduction reaching its maximum indicates the disturbing effect of roughness becomes independent of Reynolds numbers when $Re_\tau \geq 3900$. Farther from the wall, turbulence intensity increases with $Re_\tau$, particularly in the log region (as shown by the arrow), which is typical for both smooth and rough walls. Interestingly however, the mean velocity profile and inner scaled turbulence intensity shows that the two higher $Re_\tau$ cases seems to behave like a sand grain roughness (or k-type roughness).

To examine the roughness effect in the outer region, the velocity defect profiles and the turbulence intensity of smooth- and rough-wall TBLs were normalized by the outer length, $\delta_{99}$, and plotted in Figures 5(c) and (d). The velocity defect profile shows a good collapse between the rough wall cases

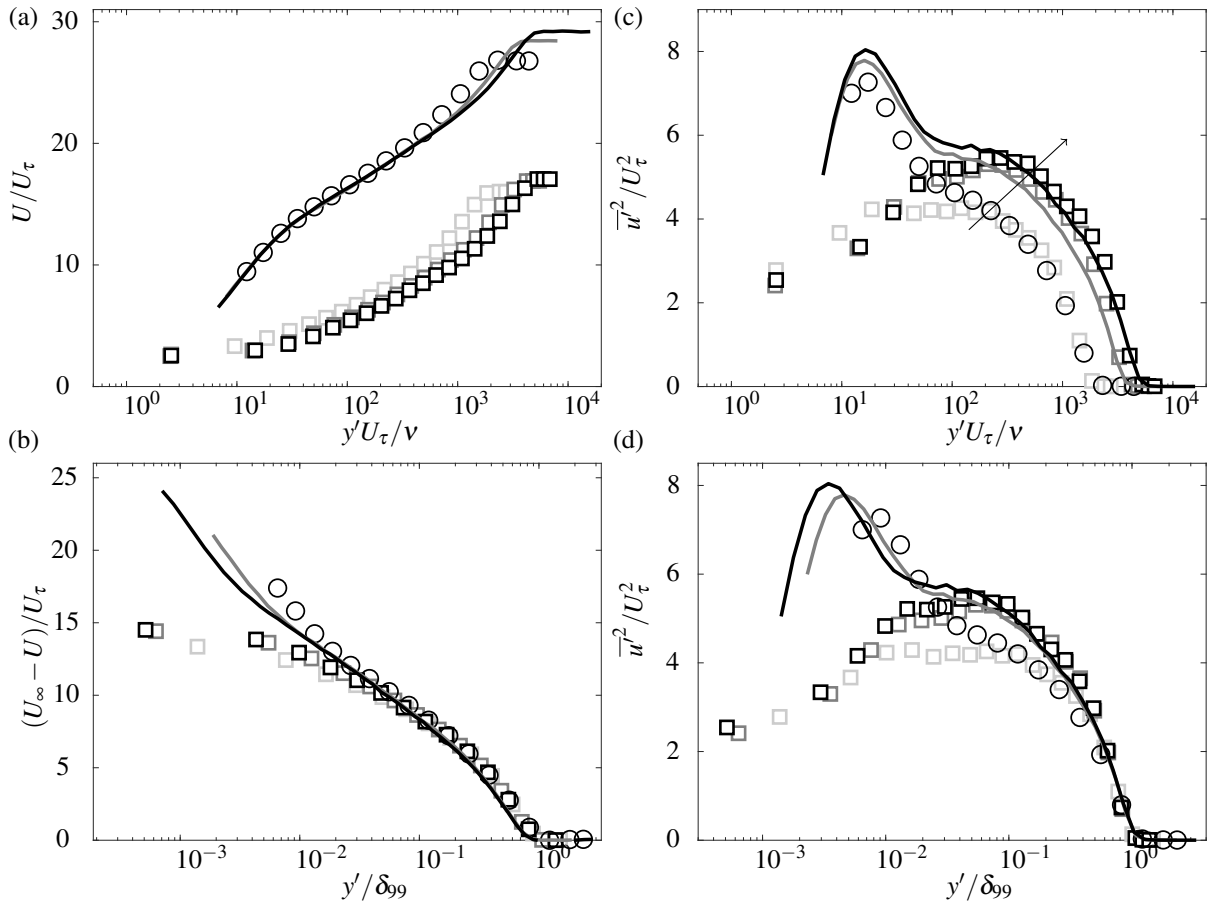


Figure 5. Comparison of the 2D roughness with $p/k = 8$ ranging from $Re_\tau = 1840 - 4950$ (refer colour codes to Table 1) and the smooth wall TBL at $Re_\tau = 1900$ (open circle) and two higher Reynolds number cases from the literature, $Re_\tau = 3500$ (grey dash line) and $Re_\tau = 4800$ (black dash line) from Marusic *et al.* (2015). Mean velocity profiles (a); inner-scaled turbulence intensity profiles (b); velocity defect profiles (c); outer-scaled turbulence intensity profiles (d).

and the smooth wall results from $y'/\delta_{99} = 0.03$. The outer scaled turbulence intensity shows a good collapse between the low $Re_\tau$ smooth- and rough-wall results ($Re_\tau \approx 1900$) from the center of the log region, $y/\delta_{99} \geq 0.2$, all the way to the outer region. For the higher $Re_\tau$ cases ($Re_\tau \approx 3470 - 4950$) the amplitude of the rough walled turbulence intensity is slightly higher than that of the smooth wall cases, spanning from the log region to half of the wake region, $0.1 \leq y/\delta_{99} \leq 0.6$. The maximum deviation of the turbulence intensity for rough wall cases and the smooth wall cases at high $Re_\tau$ is about 10% at $y/\delta_{99} \approx 0.3$. Such deviation (despite our relatively high $Re_\tau$) may be caused by the low ratio of $\delta_{99}/k \approx 53$, which is much smaller than that of Efros & Krogstad (2011) ($\delta_{99}/k \approx 130$). Hence although the velocity defect profile indicates a good agreement with the similarity hypothesis, the outer scaled turbulence intensity is slightly deviate.

The drag coefficient $C_f$ can be calculated as

$$C_f = 2(U_\tau/U_\infty)^2, \tag{4}$$

which states that the drag coefficient is related to the ratio of inner and outer velocity scales, namely $U_\tau$ and $U_\infty$. Hence, the amplitude of the free-stream edge of the normalized mean velocity profiles can reflect the drag coefficient by considering the quantity $U_\infty^+ = U_\infty/U_\tau = \sqrt{2/C_f}$. The value of $C_f$ for all rough wall cases has been summarized in Table 1. From the table we can see that the $C_f$ seems to converge at s 0.0069, indicating that rough-wall TBLs are fully-developed, and will show a similar shape in the outer region of the mean velocity and turbulence intensity profiles, scaled by the outer length, $\delta_{99}$ (Djenidi *et al.*, 2018). In addition, $\delta_{99}/k$ increases with $Re_\tau$ due to the boundary layer thickness growth, but the increase of $\delta_{99}/k$ is small when $Re_\tau \geq 3900$. The slow-growing rate of $\delta_{99}/k$ also indicates that fully-developed rough wall TBLs have sufficiently large $\delta_{99}/k$ to yield the same $C_f$. Considering the value of $C_f = 0.007$ from 2D roughness square-bar roughness with $p/k = 8$ at $Re_\tau \geq 9900$ and $\delta_{99}/k \geq 96$ (Efros & Krogstad, 2011), $C_f$ can reach its constancy at $C_f \approx 0.0069$, and the rough-wall TBL achieves its fully-developed state when $Re_\tau \geq 3900$ and $\delta_{99}/k \geq 53$.

By looking at the converges of $C_f$ and the plots in figures 5(a) and (b) where the highest $Re_\tau$ cases behave like a sand-grain roughness flow (or k-type roughness), one would suspect that the flow may indeed a k-type roughness. However we are unable to reach this conclusion, because it requires more data at higher $Re_\tau$ which is outside the range of our wind tunnel. Despite this, the data indicate all present rough-wall results are at a fully-rough regime with $\Delta U^+ > 10$. Hence, the critical $Re_\tau$ and $\delta_{99}/k$ at which the rough wall TBL over 2D square-bar roughness with $p/k = 8$ achieves a fully-developed and fully-rough regimes are 3900 and 53, respectively.

## CONCLUSION

The experimental study of rough wall TBLs consisting of spanwise square bars was performed to investigate the drag coefficient and the effects of Reynolds numbers for a 2D roughness with $p/k = 8$ at moderate Reynolds numbers. For rough wall measurements, the friction velocity $U_\tau$ is estimated by an improved technique, and the modified diagnostic plot shows agreement with the value of $\Delta U^+$ obtained from this technique. The rough wall results with $p/k = 8$ ranging from $Re_\tau = 1840 - 4950$ show a slight discrepancy for the turbulence intensity in the outer region between the smooth and rough wall cases, which extends to the middle of the wake region at $y'/\delta_{99} = 0.6$, despite the fact that the velocity defect data of the rough wall and the smooth wall collapses well. Such results prevent us to reach a conclusion whether the outer layer similarity hypothesis is preserved or not. The deviation in the outer scaled turbulence intensity is, despite our relatively high $Re_\tau$ may be caused by the relatively low ratio of $\delta_{99}/k \approx 53$. The variation of $C_f$ against $Re_\tau$ and $\delta_{99}/k$ shows that the drag coefficient for the 2D square bars roughness with $p/k = 8$ converges at 0.0069. The TBL over this 2D roughness may achieve fully-developed and fully-rough regimes at $Re_\tau = 3900$ and $\delta_{99}/k = 53$, respectively.

## ACKNOWLEDGEMENTS

The authors wish to thank their Australian Research Council (ARC) for the financial support for this research.

## REFERENCES

Adrian, R. J., Meinhart, C. D. & Tomkins, C. D. 2000 Vortex organization in the outer region of the turbulent boundary layer. *J. Fluid Mech.* **422**, 1–54.

Alfredsson, P. Henrik & Örlü, Ramis 2010 The diagnostic plot a litmus test for wall bounded turbulence data. *Eur. J. Mech. B/Fluids* **29** (6), 403–406.

Castro, Ian P., Segalini, Antonio & Alfredsson, P. Henrik 2013 Outer-layer turbulence intensities in smooth- and rough-wall boundary layers. *J. Fluid Mech.* **727**, 119–131.

Chan, C. I., Schlatter, P. & Chin, R. C. 2021 Interscale transport mechanisms in turbulent boundary layers. *J. Fluid Mech.* **921**, 13.

Chauhan, Kapil A., Monkewitz, Peter A. & Nagib, Hassan M. 2009 Criteria for assessing experiments in zero pressure gradient boundary layers. *Fluid Dyn. Res.* **41** (2).

Chauhan, Kapil A., Nagib, Hassan M. & Monkewitz, Peter A. 2007 On the composite logarithmic profile in zero pressure gradient turbulent boundary layers. *Collect. Tech. Pap. - 45th AIAA Aerosp. Sci. Meet.* **9**, 6432–6449.

Chung, Daniel, Hutchins, Nicholas, Schultz, Michael P. & Flack, Karen A. 2021 Predicting the Drag of Rough Surfaces. *Annu. Rev. Fluid Mech.* **53**, 439–471.

Clauser, Francis H. 1954 Turbulent Boundary Layers in Adverse Pressure Gradients. *J. Aeronaut. Sci.* **21** (2), 91–108.

Djenidi, L., Talluru, K. M. & Antonia, R. A. 2018 Can a turbulent boundary layer become independent of the Reynolds number? *J. Fluid Mech.* **851**, 1–22.

Efros, Vladislav & Krogstad, Per Åge 2011 Development of a turbulent boundary layer after a step from smooth to rough surface. *Exp. Fluids* **51** (6), 1563–1575.

Flack, K. A., Schultz, M. P. & Connelly, J. S. 2007 Examination of a critical roughness height for outer layer similarity. *Phys. Fluids* **19** (9), 95104.

Hutchins, N., Nickels, T. B., Marusic, I. & Chong, M. S. 2009 Hot-wire spatial resolution issues in wall-bounded turbulence. *J. Fluid Mech.* **635**, 103–136.

Jiménez, Javier 2004 Turbulent flows over rough walls. *Annu. Rev. Fluid Mech.* **36** (1), 173–196.

Kline, S. J., Reynolds, W. C., Schraub, F. A. & Runstadler, P. W. 1967 The structure of turbulent boundary layers. *J. Fluid Mech.* **30** (4), 741–773.

Krogstad, P. Å & Antonia, R. A. 1999 Surface roughness effects in turbulent boundary layers. *Exp. Fluids* **27** (5), 450–460.

Lee, Seung Hyun & Sung, Hyung Jin 2007 Direct numerical simulation of the turbulent boundary layer over a rod-roughened wall. *J. Fluid Mech.* **584**, 125–146.

Leonardi, S., Orlandi, P., Smalley, R. J., Djenidi, L. & Antonia, R. A. 2003 Direct numerical simulations of turbulent channel flow with transverse square bars on one wall. *J. Fluid Mech.* **491** (491), 229–238.

Ligrani, P. M. & Bradshaw, P. 1987 Subminiature hot-wire sensors: Development and use. *J. Phys. E.* **20** (3), 323–332.

Marusic, I., Chauhan, K. A., Kulandaivelu, V. & Hutchins, N. 2015 Evolution of zero-pressure-gradient boundary layers from different tripping conditions. *J. Fluid Mech.* **783**, 379–411.

Marusic, Ivan, Monty, Jason P., Hultmark, Marcus & Smits, Alexander J. 2013 On the logarithmic region in wall turbulence. *J. Fluid Mech.* **716**.

Monty, J. P., Allen, J. J., Lien, K. & Chong, M. S. 2011 Modification of the large-scale features of high Reynolds number wall turbulence by passive surface obtrusions. *Exp. Fluids* **51** (6), 1755–1763.

Perry, A. E. & Joubert, P. N. 1963 Rough-wall boundary layers in adverse pressure gradients. *J. Fluid Mech.* **17** (2), 193–211.

Perry, A. E. & Li, J. D. 1990 Experimental support for the attached-eddy hypothesis in zero-pressure-gradient turbulent boundary layers. *J. Fluid Mech.* **218**, 405–438.

Raupach, Michael R., Antonia, Robert Anthony & Rajagopalan, S. 1991 Rough-wall turbulent boundary layers. *Appl. Mech. Rev.* **44** (1), 1–26.

Schultz, M. P. & Flack, K. A. 2007 The rough-wall turbulent boundary layer from the hydraulically smooth to the fully rough regime. *J. Fluid Mech.* **580**, 381–405.

Schultz, M. P. & Myers, A. 2003 Comparison of three roughness function determination methods. *Exp. Fluids* **35** (4), 372–379.

Squire, D. T., Morrill-Winter, C., Hutchins, N., Schultz, M. P., Klewicki, J. C. & Marusic, I. 2016 Comparison of turbulent boundary layers over smooth and rough surfaces up to high Reynolds numbers. *J. Fluid Mech.* **795**, 210–240.

Townsend, A. A. 1974 *the Structure of Turbulent Shear Flow.*, 2nd edn. Cambridge [England] ;;New York: Cambridge University Press.

Volino, R. J., Schultz, M. P. & Flack, K. A. 2009 Turbulence structure in a boundary layer with two-dimensional roughness. *J. Fluid Mech.* **635**, 75–101.

Volino, Ralph J., Schultz, Michael P. & Flack, Karen A. 2011 Turbulence structure in boundary layers over periodic two- and three-dimensional roughness. *J. Fluid Mech.* **676**, 172–190.